



HAL
open science

Modelling of the migration of endothelial cells on bioactive micropatterned polymers

Thierry Colin, Marie-Christine Durrieu, Julie Joie, Y. Lei, Youcef Mammeri,
Clair Poignard, Olivier Saut

► **To cite this version:**

Thierry Colin, Marie-Christine Durrieu, Julie Joie, Y. Lei, Youcef Mammeri, et al.. Modelling of the migration of endothelial cells on bioactive micropatterned polymers. [Research Report] RR-7998, 2012. hal-00709993v1

HAL Id: hal-00709993

<https://inria.hal.science/hal-00709993v1>

Submitted on 19 Jun 2012 (v1), last revised 9 Jul 2012 (v3)

HAL is a multi-disciplinary open access archive for the deposit and dissemination of scientific research documents, whether they are published or not. The documents may come from teaching and research institutions in France or abroad, or from public or private research centers.

L'archive ouverte pluridisciplinaire **HAL**, est destinée au dépôt et à la diffusion de documents scientifiques de niveau recherche, publiés ou non, émanant des établissements d'enseignement et de recherche français ou étrangers, des laboratoires publics ou privés.



Modelling of the migration of endothelial cells on bioactive micropatterned polymers

Thierry Colin, Marie-Christine Durrieu, Julie Joie , Yifeng Lei ,
Youcef Mammeri, Clair Poignard , Olivier Saut

**RESEARCH
REPORT**

N° 7998

June 2012

Project-Teams MC2



Modelling of the migration of endothelial cells on bioactive micropatterned polymers

Thierry Colin ^{*}, Marie-Christine Durrieu[†], Julie Joie [‡], Yifeng
Lei [§], Youcef Mammeri[¶], Clair Poignard [¶], Olivier Saut^{||}

Project-Teams MC2

Research Report n° 7998 — June 2012 — 23 pages

Abstract: In this paper a macroscopic model describing endothelial cells migration on bioactive micropatterned polymers is presented. It is based on a system of partial differential equations of Patlak-Keller-Segel type that describes the evolution of the cell densities. The model is studied mathematically and numerically. We prove existence and uniqueness results of the solution to the differential system and also that fundamental physical properties such as mass conservation, positivity and boundedness of the solution are satisfied. The numerical study allows us to show that the model behaves in good agreement with the experiments.

Key-words: Cell migration modelling, Chemotaxis, Non-linear P.D.E

* Univ. Bordeaux, IMB, UMR 5251, F-33400 Talence, France.

† CNRS, IECB, UMR 5248, F-33607 PESSAC, France

‡ Univ. Bordeaux, IMB, UMR 5251, F-33400 Talence, France

§ Univ. Bordeaux, IECB, UMR 5248, F-33607 PESSAC, France

¶ INRIA, IMB, UMR 5251, F-33400 Talence, France.

|| CNRS, IMB, UMR 5251, F-33400 Talence, France.

**RESEARCH CENTRE
BORDEAUX – SUD-OUEST**

351, Cours de la Libération
Bâtiment A 29
33405 Talence Cedex

Modelling of the migration of endothelial cells on bioactive micropatterned polymers

Résumé : In this paper a macroscopic model describing endothelial cells migration on bioactive micropatterned polymers is presented. It is based on a system of partial differential equations of Patlak-Keller-Segel type that describes the evolution of the cell densities. The model is studied mathematically and numerically. We prove existence and uniqueness results of the solution to the differential system and also that fundamental physical properties such as mass conservation, positivity and boundedness of the solution are satisfied. The numerical study allows us to show that the model behaves in good agreement with the experiments.

Mots-clés : Cell migration modelling, Chemotaxis, Non-linear P.D.E

Contents

1	Introduction	4
2	Description of the model and main result	5
2.1	Statement of the equations	6
2.2	Main theoretical result	7
3	Theoretical study of the model	7
3.1	Kernels of the operators	8
3.2	Local existence	10
3.2.1	Definition of the appropriate functional space \mathcal{X}_M^T	10
3.2.2	Contraction mappings	11
3.3	Mass conservation and global existence	12
4	Numerical results	15
4.1	Approximation of the problem	15
4.2	Mathematical behavior of the model	16
4.3	Behavior on realistic benchmarks	16
4.3.1	Behavior on thin strips	16
4.3.2	Behavior on large strips	18
4.3.3	Influence of the number of strips on the migration	20
5	Conclusion	21

1 Introduction

Tissue engineering is the use of combination of cells, engineering, materials, and suitable biochemical factors to improve or replace biological functions [26]. Tissue engineering has been quickly developing since the 1990s [26]. However, the major roadblock for engineering large tissues is the lack of functional microvasculature networks, which provide nutrients and oxygen for tissue survival and remove the waste product from metabolism [18]. The lack of vascularization has hampered the survival of engineered tissues after implantation [18]. Researchers rely on the increasing knowledge of angiogenic and vasculogenic processes to stimulate vascular network formation [32, 31]. This complex process of new blood vessel formation is orchestrated by the interaction between endothelial cells (ECs) and their neighboring mural cells via a complex network of intracellular signaling mechanisms [28, 17]. Ever since the introduction of the *in vitro* model of angiogenesis [11], there has been great research interest to understand the intricate process of tube formation. Although many efforts have been made, the mechanism associated with angiogenesis and vascularization is poorly understood. A deeper comprehension of cells-biomaterials interaction is required for basic understanding of angiogenesis and vascularization in tissue engineering [5].

One strategy in developing clinical implants is therefore to use bioactive materials which can either elicit a regenerative response at the site of damage *in vivo* or be used to grow tissue *in vitro* for subsequent implantation [2, 23]. Different bioactive ligands have been used to study their effects on cell functions for a better understanding of vascularization [31]. In the aim at promoting angiogenesis in the case of tissue engineering or inhibiting angiogenesis in the case of cancer, it is now important to understand the mechanisms that regulate lumen formation. Successful micropatterning of cells is becoming a key component of this field [16]. Researchers are now interested in the behavior of cells on substrates that have been patterned by micro/nanofabrication [10, 27]. It is known that cell positioning and physiology can be controlled by the substrate on which the cells adhere [6]. In our study, using cell adhesion peptides micropatterned onto material, we observed a tube-like formation in comparison to virgin material or homogeneously grafted materials [22, 23].

Experimental studies using micropatterned substrates revealed that the cell migration is governed by the geometry of the patterns (size of patterns and distance between patterns). Endothelial cells so cultured form extensive cell-cell interactions. Accumulation of endothelial cells junctions implies that some cells form tube-like structures. The goal of the present paper is to provide a model that describes such results.

Adhesive areas are composed of cell adhesion peptides or growth factors peptides that make the cells adhere. These areas are surrounded by non-adhesive areas [22]. We assume (and this is actually confirmed by experiments) that active principles (cell adhesion peptides or growth factors) are not diffusing spatially. Therefore endothelial cells outside adhesive areas have no mean to "feel" directly these areas. They find out these areas indirectly. We do not consider the influence of nutrients and assume that cells obtain enough nutrients from the material (due to grafted active principles onto material). Endothelial cells are seeded onto micropatterned bioactive materials during several hours, then they are washed out. Only the adhered endothelial cells remain on material. The initial density of cells is around 40 000 cells per cm^2 . At the beginning of the experiments, during the migration phase we observe that cells have a random motility and stop on adhesive areas. Moreover the attraction of endothelial cells on adhesive areas seems to be higher than the one of cells outside these areas. Experiments show that endothelial cells are grouping together along the micropatterns. According to pattern size, endothelial cells line their cytoskeleton to adjust it with the adhesive area. One can also notice that, with micropatterns of 10 μm thin strips, tubes containing a central lumen may appear [23, 7]. In

other words, blood vessels are created from an initial random density of endothelial cells. Such phenomenon is not observed with larger strips [7, 20, 25].

To illustrate these experiments, we present in Fig.1 pictures of the micropatterned bioactive materials at the end of the migration step. Two different micropatterns are considered: on Fig.1(a) thin adhesive areas (bioactive pattern size: $10\ \mu\text{m}$ and distance between patterns: $100\ \mu\text{m}$) have been used, whereas Fig.1(b) shows the end of the migration on large strips (bioactive pattern size: $300\ \mu\text{m}$ and distance between patterns: $100\ \mu\text{m}$). For a detailed description of such experiences, one may refer to [22, 23].

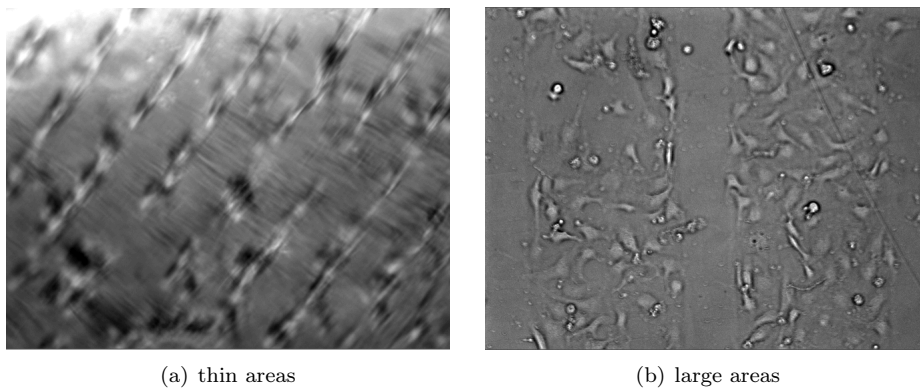


Figure 1: Endothelial cells alignment onto micropatterned polymer (PET) ($10\ \mu\text{m}$ (A) and $300\ \mu\text{m}$ (B) stripes of SVVYGLR peptides) [22]. The distance between bioactive patterns is $100\ \mu\text{m}$.

We observed that for the largest adhesive areas the adhered cells density is smaller than for thin strips. Therefore the geometries of the micropatterns play a crucial role in the endothelial cells migration and then in the formation of new vessel.

In this paper we are interested in understanding how these patterns (size and distance between microfeatures) do influence endothelial cells migration. The model we present here is a continuous Patlak-Keller-Segel type model [1, 13, 21, 30]. The chemotaxis term takes the cell-cell interactions into account instead of the cell-chemical attractant interactions. We show that this new model based on a system of coupled partial differential equations conserves the mass and existence and uniqueness results of weak solution hold. We also provide numerical results in accordance with the experiments, which ensures the validity of our model. Moreover, these simulations allow us to obtain informations on the influence of the geometry and of the initial concentration of cells on the migration of the cells.

The outline of the article is the following. In section 2 we describe the mathematical model and we state the main result of global existence and uniqueness of the weak solution to the P.D.E system. Section 3 is devoted to proof the main theorem. We then provide numerical results in section 4 in order to compare the simulations to the experiments.

2 Description of the model and main result

In this section we describe the Patlak-Keller-Segel type continuous model we study throughout the paper. The model is composed of a diffusion term coupled with a reaction term, which describes the effect of the chemoattractants, which themselves satisfy a diffusion equation.

Various continuous models of Patlak and Keller-Segel type have been used to describe cell motility. Typically, the governing equations of these models are written in the following general form: on a domain $\Omega \subset \mathbb{R}^n$

$$\begin{aligned}\partial_t u &= \nabla \cdot (D_1(u, v)\nabla u - \chi(u, v)u\nabla v) + f(u, v) && \text{on } \Omega \\ \partial_t v &= \nabla \cdot (D_2(u, v)\nabla v) + g(u, v) - h(u, v)v && \text{on } \Omega,\end{aligned}$$

where u denotes the cells density, v is the chemical signal concentration. The diffusive terms takes the random motility of the cells into account, whereas the advection describes the influence of the chemical signal on the motion of the cells. The two corresponding diffusion parameters are denoted by D_1 and D_2 while χ is the chemotaxis coefficient. The function f describes the growth and the death of cells, whereas g and h are the production and degradation of the chemotactic signal. These equations have been theoretically studied [3, 4, 8, 12, 14, 33] for several years. Based on this extensive literature we provide a slightly modified model to describe the cell migration on bioactive micropatterns.

2.1 Statement of the equations

According to the experiments, the behavior of the cells is drastically different on the adhesive area and outside this area. Actually, outside the adhesive strip the cells seem to attract each other (probably thanks to the chemoattractant they produce) and also diffuse in the domain, but as soon as they reach the adhesive strip they seem stuck on the strip and then they diffuse only on this area, ignoring the outer cells. Moreover it seems that the production of chemoattractant of the cells located on the adhesive strip is bigger than outside.

Since there is no clear understanding of the way that endothelial cells communicate, we chose to consider the chemotaxis term as the attraction between endothelial cells (and we do not consider any gradient of concentration of the chemoattractant).

Based on these assumptions, we derive the following model. Consider a domain Ω composed by the adhesive areas, denoted $\tilde{\Omega}$, and the non-adhesive areas $\Omega \setminus \tilde{\Omega}$, both domains being bounded domains with smooth boundary.

Two different types of endothelial cells are considered. We denote by $u_1(t, x, y)$ the density of endothelial cells, at any point (x, y) and time t , that can freely move (*i.e.* they have yet to move over adhesion proteins). Cells that are adhering on the substrate are tracked through their density u_2 . The function v represents the density of the chemoattractant. The equations governing the endothelial cells migration are given for $t > 0$ by

$$\partial_t u_1 = d_1 \Delta u_1 - \lambda \mathbf{1}_{\tilde{\Omega}} u_1 (1 - u_2) - \nabla \cdot (\chi(u_1, v) u_1 \nabla v), \quad \text{in } \Omega, \quad (1a)$$

$$\partial_t u_2 = d_2 \Delta u_2 + \lambda \mathbf{1}_{\tilde{\Omega}} u_1 (1 - u_2), \quad \text{in } \tilde{\Omega}, \quad (1b)$$

$$\partial_t v = \Delta v - \eta v + \gamma_1 u_1 + \gamma_2 u_2, \quad \text{in } \Omega, \quad (1c)$$

with the homogeneous boundary conditions on $\partial\Omega$ and $\partial\tilde{\Omega}$:

$$\partial_n u_1|_{\partial\Omega} = 0, \quad \partial_n u_2|_{\partial\tilde{\Omega}} = 0, \quad \partial_n v|_{\partial\Omega} = 0, \quad (1d)$$

and with the initial conditions $(u_1^0, u_2^0, 0)$

$$u_1|_{t=0} = u_1^0, \quad u_2|_{t=0} = u_2^0, \quad v|_{t=0} = 0. \quad (1e)$$

We then denote by u the sum

$$u(t, x) = u_1(t, x) + u_2(t, x), \quad t \geq 0, \quad x \in \Omega,$$

where u_2 is extended by 0 in $\Omega \setminus \tilde{\Omega}$.

The parameters $d_1, d_2, \eta, \gamma_1, \gamma_2$ and λ are strictly positive and they will be fitted by the experiments in a forthcoming work, but we consider here that they are given constants. The coefficients d_1 and d_2 denote the diffusion coefficients of the cells u_1 and u_2 respectively. The coefficient $\eta > 0$ is the self-degradation rate of the chemoattractant produced by the cells, while the coefficients γ_1 and γ_2 are the coefficients of the production of the chemoattractant respectively for the cell u_1 and u_2 . The parameter λ is the rate for the cell u_1 to become u_2 as soon as u_1 lies in the micropatterns. The two first equations describe the migration of the cells on Ω . Outside the strips, endothelial cells diffuse and attract the neighboring cells via the chemotaxis sensitivity function :

$$\chi(u_1, v) = \chi^0 \frac{v}{1 + |v|} (1 - u_1), \quad \text{with } \chi^0 > 0.$$

Here above, χ^0 is a chemotaxis parameter, and the term $(1 - u_1)$ is settled to prevent the overcrowding of the cells u_1 . Endothelial cells once they reach the adhesive area $\tilde{\Omega}$ are captured and then diffuse only in the strip. This is handled by the penalty term $-\lambda \mathbb{1}_{\tilde{\Omega}} u_1 (1 - u_2)$. Cells on the strips still have a random motility and their concentration grows up as the term $\lambda \mathbb{1}_{\tilde{\Omega}} u_1 (1 - u_2)$, where $1 - u_2$ prevents the blow-up of u_2 in equation (1b). The third equation describes the production of the chemoattractant by the cells. Since the cells on the strip seem to be more attractive, we suppose that the production coefficients checks $0 < \gamma_1 < \gamma_2$. We also add a degradation coefficient $\eta > 0$ describing the metabolization of the chemoattractant.

2.2 Main theoretical result

We have the following theorem which is a straightforward consequence of the results of the next section 3:

Theorem 2.1. *Let $d_1, d_2, \eta, \gamma_1, \gamma_2$ and λ be strictly positive constants. Suppose that the initial data $(u_1^0, u_2^0) \in L^\infty(\Omega) \times L^\infty(\tilde{\Omega})$ are such that*

$$\forall x \in \Omega, \quad 0 \leq u_1^0(x) \leq 1, \quad \forall x \in \tilde{\Omega}, \quad 0 \leq u_2^0(x) \leq 1.$$

There exists a unique weak solution (u_1, u_2, v) to problem (1) such that

$$(u_1, u_2, v) \in L^\infty([0, +\infty); L^\infty(\Omega)) \times L^\infty([0, \infty); L^\infty(\tilde{\Omega})) \times L^\infty([0, \infty); L^\infty(\Omega)),$$

and for almost any $t > 0$

$$0 \leq u_1(t, \cdot) \leq 1, \quad 0 \leq u_2(t, \cdot) \leq 1, \quad \text{and} \quad 0 \leq v(t, \cdot) \leq \frac{1}{\eta} (\gamma_1 + \gamma_2).$$

The next section is devoted to prove this theorem. The proof is based on Gaussian upper bounds for heat kernels [29]–[35].

3 Theoretical study of the model

In this section we study the mathematical properties of the model. Throughout this section we suppose that $\tilde{\Omega}$ and Ω are smooth domains of \mathbb{R}^2 . We remind that d_1, d_2 and η are strictly positive coefficients.

3.1 Kernels of the operators

The aim of this paragraph is to define and provide estimates of the kernels of the operators $\partial_t - \Delta + \eta$ and $\partial_t - d_1 \Delta$ on Ω and for the kernel of $\partial_t - d_2 \Delta$ on $\tilde{\Omega}$, with homogeneous Neumann conditions respectively on $\partial\Omega$ and $\partial\tilde{\Omega}$.

Definition 3.1. *The kernels \mathcal{B} , \mathcal{G} and $\tilde{\mathcal{G}}$ of the respective operators $\partial_t - \Delta + \eta$, $\partial_t - d_1 \Delta$ on Ω , and $\partial_t - d_2 \Delta$ on $\tilde{\Omega}$, all with homogeneous Neumann conditions, are respectively defined by*

$$\forall (x, y) \in \Omega, \quad \lim_{t \rightarrow 0^+} \mathcal{B}(t, x, y) = \delta_y(x),$$

and for any $(t, y) \in (0, \infty) \times \Omega$,

$$\begin{cases} \partial_t \mathcal{B}(t, x, y) = \Delta \mathcal{B}(t, x, y) - \eta \mathcal{B}(t, x, y), & \forall x \in \Omega, \\ \partial_{\mathbf{n}} \mathcal{B}(t, x_{\partial\Omega}, y) = 0, & \forall x_{\partial\Omega} \in \partial\Omega, \end{cases} \quad (2a)$$

for \mathcal{B} , while \mathcal{G} is given by

$$\forall (x, y) \in \Omega, \quad \lim_{t \rightarrow 0^+} \mathcal{G}(t, x, y) = \delta_y(x), \quad (3a)$$

and for any $(t, y) \in (0, \infty) \times \Omega$,

$$\begin{cases} \partial_t \mathcal{G}(t, x, y) = d_1 \Delta \mathcal{G}(t, x, y), & \forall x \in \Omega, \\ \partial_{\mathbf{n}} \mathcal{G}(t, x_{\partial\Omega}, y) = 0, & \forall x_{\partial\Omega} \in \partial\Omega, \end{cases} \quad (3b)$$

and $\tilde{\mathcal{G}}$ is the solution to

$$\forall (x, y) \in \tilde{\Omega}, \quad \lim_{t \rightarrow 0^+} \tilde{\mathcal{G}}(t, x, y) = \delta_y(x), \quad (4a)$$

and for any $(t, y) \in (0, \infty) \times \tilde{\Omega}$,

$$\begin{cases} \partial_t \tilde{\mathcal{G}}(t, x, y) = d_2 \Delta \tilde{\mathcal{G}}(t, x, y), & \forall x \in \tilde{\Omega}, \\ \partial_{\mathbf{n}} \tilde{\mathcal{G}}(t, x_{\partial\tilde{\Omega}}, y) = 0, & \forall x_{\partial\tilde{\Omega}} \in \partial\tilde{\Omega}. \end{cases} \quad (4b)$$

Note that the above kernels are symmetric in their second and third variables.

Proposition 1. *For any $y \in \Omega$ (respectively for any $y \in \tilde{\Omega}$), we have the following estimates for positive constants C_Ω and $C_{\tilde{\Omega}}$, which depend on the domain Ω and $\tilde{\Omega}$ respectively:*

$$\|\mathcal{G}(t, \cdot, y)\|_{L^1(\Omega)} \leq C_\Omega, \quad (5a)$$

$$\|\tilde{\mathcal{G}}(t, \cdot, y)\|_{L^1(\tilde{\Omega})} \leq C_{\tilde{\Omega}}, \quad (5b)$$

$$\|\mathcal{B}(t, \cdot, y)\|_{L^1(\Omega)} \leq C_\Omega, \quad (5c)$$

and gradient estimates hold too:

$$\|\nabla_x \mathcal{G}(t, \cdot, y)\|_{L^1(\Omega)} \leq C_\Omega \max(1, t^{-3/4}), \quad (6a)$$

$$\|\nabla_x \tilde{\mathcal{G}}(t, \cdot, y)\|_{L^1(\tilde{\Omega})} \leq C_{\tilde{\Omega}} \max(1, t^{-3/4}), \quad (6b)$$

$$\|\nabla_x \mathcal{B}(t, \cdot, y)\|_{L^1(\Omega)} \leq C_\Omega \max(1, t^{-3/4}). \quad (6c)$$

In addition due to the boundedness of Ω , we also have

$$\|\nabla_y \mathcal{G}(t, \cdot, y)\|_{L^1(\Omega)} \leq C_\Omega \max(1, t^{-3/4}), \quad (7a)$$

$$\|\nabla_y \tilde{\mathcal{G}}(t, \cdot, y)\|_{L^1(\Omega)} \leq C_{\tilde{\Omega}} \max(1, t^{-3/4}), \quad (7b)$$

$$\|\nabla_y \mathcal{B}(t, \cdot, y)\|_{L^1(\Omega)} \leq C_\Omega \max(1, t^{-3/4}). \quad (7c)$$

Proof. Obviously the coefficients of diffusion d_1 and d_2 , since they are strictly positive constants do not play a crucial role, and can be supposed to be 1, after an appropriate rescaling of the time variable t . Moreover it is sufficient to prove the above estimates for the heat kernel \mathcal{G} , since

$$\mathcal{B} = e^{-\eta t} \mathcal{G}.$$

For $t \geq 1$, estimates (3.2)–(3.3) of [35] straightforwardly provide the result. Suppose that $0 < t \leq 1$. Estimates (5a) easily come from Theorem 6.10 pp 171 of [29], since for any $x \in \Omega$,

$$0 \leq \frac{1}{\sqrt{t}} \int_{\Omega} e^{-|x-y|^2/t} dy \leq 2\pi.$$

Estimates (6a) are consequences of the section 6.6 entitled Weighted Gradient Estimates and in particular Theorem 6.19 p 185 [29]. Actually by Cauchy-Schwarz inequality

$$\begin{aligned} \|\nabla_x \mathcal{G}(t, \cdot, y)\|_{L^1(\Omega)}^2 &\leq \int_{\Omega} |\nabla_x \mathcal{G}(t, \cdot, y)|^2 e^{2\beta|x-y|^2/t} dy \int_{\Omega} e^{-2\beta|x-y|^2/t} dy \\ &\leq Ct^{-2} e^{ct} \int_{\Omega} e^{-2\beta|x-y|^2/t} dy, \\ &\leq 2\pi Ct^{-3/2} e^{ct} \leq Ct^{-3/2}, \end{aligned}$$

hence the estimates (6a).

Now let $\phi \in L^\infty(\Omega)$, by estimates (6a) and since the measure $|\Omega|$ of Ω is bounded we infer

$$\begin{aligned} \int_{\Omega} |\phi(y)| \int_{\Omega} |\nabla_y \mathcal{G}(t, x, y)| dx dy &= \int_{\Omega \times \Omega} |\phi(y)| |\nabla_y \mathcal{G}(t, x, y)| dy dx, \\ &\leq \|\phi\|_{L^\infty(\Omega)} \int_{\Omega} \|\nabla_y \mathcal{G}(t, x, \cdot)\|_{L^1(\Omega)} dx, \\ &\leq |\Omega| Ct^{-3/4} \|\phi\|_{L^\infty(\Omega)}, \end{aligned}$$

hence estimates (7a), which ends the proof of the proposition. \square

Remark 1. *The above estimates are probably not optimal, since for the half-plane the heat kernel write:*

$$\mathcal{G}(t, x, y) = \frac{1}{4\pi t} \left(e^{|x-y|^2/(4t)} + e^{|x-y^c|^2/(4t)} \right), \quad \text{where } y^c = (y_1, -y_2),$$

and therefore the power $t^{-3/4}$ has to be replaced by $t^{-1/2}$ similarly to the heat kernel of the whole plane \mathbb{R}^2 . However these results are sufficient to prove existence and uniqueness of the solution to problem (1).

Corollary 1. *In particular, for $T > 0$, and for any $\phi \in L^\infty([0, T]; L^\infty(\Omega))$ the solution to the following problem:*

$$\begin{cases} \partial_t u = \Delta u - \eta u + \phi(t, \cdot), & \text{in } \Omega, \\ \partial_n u|_{\partial\Omega} = 0, \quad u|_{t=0} = 0, \end{cases} \quad (8)$$

satisfies almost everywhere in $(0, T) \times \Omega$:

$$|\nabla u(t, \cdot)| \leq C_\Omega t^{1/4} \sup_{s \in (0, T)} \|\phi(s, \cdot)\|_{L^\infty(\Omega)}. \quad (9)$$

Proof. Since

$$u(t, \cdot) = \int_0^t \int_\Omega \mathcal{B}(t-s, \cdot, y) \phi(s, y) dy$$

and thus

$$\begin{aligned} |\nabla u(t, x)| &\leq \int_0^t \int_\Omega |\nabla_x \mathcal{B}(t-s, x, y) \phi(s, y)| dy \\ &\leq \sup_{s \in (0, T)} \|\phi(s, \cdot)\|_{L^\infty(\Omega)} \int_0^t \|\nabla_x \mathcal{B}(t-s, x, \cdot)\|_{L^1(\Omega)}, \end{aligned}$$

hence inequality (9). □

3.2 Local existence

Using the above appropriate kernels, we deduce that a weak solution to problem (1) writes:

$$\begin{aligned} u_1(t, x) &= \int_\Omega \mathcal{G}(t, x, y) u_1^0(y) dy - \lambda \int_0^t \int_\Omega \tilde{\mathcal{G}}(t-s, x, y) u_1(s, y) (1-u_2)(s, y) dy ds \\ &\quad + \int_0^t \int_\Omega u_1(s, y) \chi(u_1, v)(s, y) \nabla_y \mathcal{G}(t-s, x, y) \cdot \nabla v(s, y) dy ds, \end{aligned} \quad (10a)$$

$$u_2(t, x) = \int_{\tilde{\Omega}} \tilde{\mathcal{G}}(t, x, y) u_2^0(y) dy + \lambda \int_0^t \int_{\tilde{\Omega}} \tilde{\mathcal{G}}(t-s, x, y) u_1(s, y) (1-u_2)(s, y) dy ds, \quad (10b)$$

$$v(t, x) = \int_0^t \int_\Omega \mathcal{B}(t-s, x, y) (\gamma_1 u_1(s, y) + \gamma_2 u_2(s, y)) dy ds. \quad (10c)$$

In this paragraph we aim at proving a local-existence result.

3.2.1 Definition of the appropriate functional space \mathcal{X}_M^T

Let M be a strictly positive constant, and let $T > 0$ that will be chosen later. We define the functional space \mathcal{X}_M^T as

$$\mathcal{X}_M^T = \left\{ \Lambda \in L^\infty([0, T]; L^\infty(\Omega)) : \sup_{t \in [0, T]} \|\Lambda(t, \cdot)\|_{L^\infty(\Omega)} \leq M \right\}.$$

Let \mathcal{L} be the linear operator defined on $\mathcal{X}_M^T \times \mathcal{X}_M^T$ by

$$\mathcal{L} : (\nu_1, \nu_2) \mapsto \int_0^t \int_\Omega \mathcal{B}(t-s, \cdot, y) (\gamma_1 \nu_1(s, y) + \gamma_2 \nu_2(s, y)) dy ds.$$

Using estimates (5a)–(6a) we infer that for any $(\nu_1, \nu_2) \in \mathcal{X}_M^T \times \mathcal{X}_M^T$:

$$\begin{aligned} \|\mathcal{L}(\nu_1, \nu_2)(t, \cdot)\|_{L^\infty(\Omega)} &\leq C_\Omega(\gamma_1 + \gamma_2)M, \\ \|\nabla \mathcal{L}(\nu_1, \nu_2)(t, \cdot)\|_{L^\infty(\Omega)} &\leq C_\Omega(\gamma_1 + \gamma_2)Mt^{1/4}. \end{aligned} \quad (11)$$

Define now the operator \mathcal{T} on $\mathcal{X}_M^T \times \mathcal{X}_M^T$ by

$$\mathcal{T} : (\nu_1, \nu_2) \mapsto \left((\mathcal{T}_1 - \mathcal{T}_2)(\nu_1, \nu_2), \mathcal{T}_2(\nu_1, \nu_2) \right),$$

where \mathcal{T}_1 is the operator defined on $\mathcal{X}_M \times \mathcal{X}_M^T$ by

$$\mathcal{T}_1(\nu_1, \nu_2) = \int_0^t \int_\Omega \nu_1 \chi(\nu_1, \mathcal{L}(\nu_1, \nu_2)) \nabla_y \mathcal{G}(t-s, \cdot, y) \cdot \nabla_y \mathcal{L}(\nu_1, \nu_2) dy ds,$$

and \mathcal{T}_2 is defined by

$$\mathcal{T}_2(\nu_1, \nu_2) = \lambda \int_0^t \int_{\tilde{\Omega}} \tilde{\mathcal{G}}(t-s, x, y) \nu_1(s, y) (1 - \nu_2)(s, y) dy ds.$$

Remark 2. Proving that \mathcal{T} is a contraction mapping from $\mathcal{X}_M^T \times \mathcal{X}_M^T$ onto itself for small enough time T will then ensure the local existence of the weak solution given by (10) to problem (1).

3.2.2 Contraction mappings

Proposition 2. The operators \mathcal{T} is a contraction mapping from $\mathcal{X}_M^T \times \mathcal{X}_M^T$ onto itself for T small enough.

Proof. The proof is based on the properties of the kernel \mathcal{B} , \mathcal{G} and $\tilde{\mathcal{G}}$ given by Proposition 1. Thanks to estimate (5a) we deduce for any $(\nu_1, \nu_2) \in \mathcal{X}_M^T \times \mathcal{X}_M^T$:

$$\|\mathcal{T}_2(\nu_1, \nu_2)\|_{L^\infty(\tilde{\Omega})} \leq C_\Omega \lambda M (1 + M) T,$$

hence for T small enough \mathcal{T}_2 maps $\mathcal{X}_M^T \times \mathcal{X}_M^T$ onto \mathcal{X}_M^T . Moreover using inequality:

$$|\nu_1(1 - \nu_2) - \mu_1(1 - \mu_2)| \leq (1 + |\nu_2|)|\nu_1 - \mu_1| + |\nu_2||\mu_1 - \mu_2|,$$

we infer for T small enough the operator \mathcal{T}_2 is a contraction mapping from $\mathcal{X}_M^T \times \mathcal{X}_M^T$ onto \mathcal{X}_M^T .

Prove now that \mathcal{T}_1 is a contraction mapping from $\mathcal{X}_M^T \times \mathcal{X}_M^T$ onto \mathcal{X}_M^T . First observe that for any $s \in \mathbb{R}$, $|s|/(1 + |s|) \leq 1$ hence for any $\nu_1 \in \mathcal{X}_M^T$, for any $s \in \mathbb{R}$,

$$\|\chi_1(\nu_1, s)(t, \cdot)\|_{L^\infty(\Omega)} \leq \chi^0(1 + M), \quad \text{for almost any } t \in (0, T),$$

hence for any $(\nu_1, \nu_2) \in \mathcal{X}_M^T \times \mathcal{X}_M^T$

$$\|\chi_1(\nu_1, \mathcal{L}(\nu_1, \nu_2))(t, \cdot)\|_{L^\infty(\Omega)} \leq \chi^0(1 + M), \quad \text{for almost any } t \in (0, T),$$

and thanks to estimates (6a)–(11)

$$|\mathcal{T}_1(\nu_1, \nu_2)(t, \cdot)| \leq C_\Omega (\gamma_1 + \gamma_2) \chi^0(1 + M) M^2 \sqrt{T}.$$

This implies that for T small enough \mathcal{T}_1 maps $\mathcal{X}_M^T \times \mathcal{X}_M^T$ onto \mathcal{X}_M^T . In addition observe that for two couples (ν_1, ν_2) and (μ_1, μ_2) belonging to $\mathcal{X}_M^T \times \mathcal{X}_M^T$ we have

$$\begin{aligned} \mathcal{T}_1(\nu_1, \nu_2) - \mathcal{T}_1(\mu_1, \mu_2) &= \int_0^t \int_{\Omega} (\nu_1 - \mu_1) \chi^{\nu_1, \nu_2} \nabla_y \mathcal{G}(t-s, \cdot, y) \cdot \nabla_y \mathcal{L}(\nu_1, \nu_2) dy ds, \\ &+ \int_0^t \int_{\Omega} \mu_1 \chi^{\nu_1, \nu_2} \nabla_y \mathcal{G}(t-s, \cdot, y) \cdot \nabla_y \mathcal{L}(\nu_1 - \mu_1, \nu_2 - \mu_2) dy ds, \\ &+ \int_0^t \int_{\Omega} \mu_1 (\chi^{\nu_1, \nu_2} - \chi^{\mu_1, \mu_2}) \nabla_y \mathcal{G}(t-s, \cdot, y) \cdot \nabla_y \mathcal{L}(\mu_1, \mu_2) dy ds, \end{aligned}$$

where to simplify notations we have denoted by χ^{ν_1, ν_2} the function

$$\chi^{\nu_1, \nu_2} = \chi(\nu_1, \mathcal{L}(\nu_1, \nu_2)),$$

and similarly for χ^{μ_1, μ_2} . According to estimate (6a) and thanks to the definition of \mathcal{L} we infer

$$\|\nabla_y \mathcal{L}(\nu_1 - \mu_1, \nu_2 - \mu_2)\| \leq C_{\Omega} (\gamma_1 + \gamma_2) t^{1/4} (\|\nu_1 - \mu_1\|_{L^{\infty}(\Omega)} + \|\nu_2 - \mu_2\|_{L^{\infty}(\Omega)}).$$

Moreover, observing that

$$\begin{aligned} \chi^{\nu_1, \nu_2} - \chi^{\mu_1, \mu_2} &= \chi^0 \frac{\mathcal{L}(\nu_1, \nu_2)}{1 + |\mathcal{L}(\nu_1, \nu_2)|} (\mu_1 - \nu_1) \\ &+ \chi^0 (1 - \mu_1) \left(\frac{\mathcal{L}(\nu_1, \nu_2)}{1 + |\mathcal{L}(\nu_1, \nu_2)|} - \frac{\mathcal{L}(\mu_1, \mu_2)}{1 + |\mathcal{L}(\mu_1, \mu_2)|} \right), \end{aligned}$$

we deduce from estimates (5a)–(6a)–(7a) and (11) that there exists a constant $C > 0$ which depends on M , and on the parameters χ^0 , γ_1 , γ_2 , λ such that

$$\|\mathcal{T}_1(\nu_1, \nu_2) - \mathcal{T}_1(\mu_1, \mu_2)\|_{L^{\infty}(\Omega)} \leq C\sqrt{T},$$

which ensures the strict contractility of \mathcal{T}_1 for T small enough, and therefore \mathcal{T} is a strict contraction from $\mathcal{X}_M^T \times \mathcal{X}_M^T$ onto itself. \square

The Picard fixed point theorem straightforwardly implies the following theorem of existence and uniqueness for small time.

Theorem 3.2. *Let $(u_1^0, u_2^0) \in L^{\infty}(\Omega) \times L^{\infty}(\tilde{\Omega})$. Then for T small enough there exists a unique weak solution (u_1, u_2, v) to (1) such that*

$$(u_1, u_2, v) \in L^{\infty}([0, T]; L^{\infty}(\Omega)) \times L^{\infty}([0, T]; L^{\infty}(\tilde{\Omega})) \times L^{\infty}([0, T]; L^{\infty}(\Omega)).$$

3.3 Mass conservation and global existence

We first observe that the total mass of cells is conserved.

Proposition 3. *Let $(u_1^0, u_2^0) \in L^{\infty}(\Omega) \times L^{\infty}(\tilde{\Omega})$ and let T small enough so that a weak solution (10) to (1) exists. Then for any $t \in [0, T]$*

$$\int_{\Omega} u(t, x) dx = \int_{\Omega} (u_1 + \mathbb{1}_{\tilde{\Omega}} u_2)(t, x) dx = \int_{\Omega} u_1^0 dx + \int_{\tilde{\Omega}} u_2^0 dx$$

Proof. Actually integrating (1a) and (1b) respectively and summing the integrands imply, since $\partial_n u_1|_{\partial\Omega}$, $\partial_n u_2|_{\partial\tilde{\Omega}}$ and $\partial_n v|_{\partial\Omega}$ vanish

$$\partial_t \int_{\Omega} u(x) dx = \partial_t \int_{\Omega} (u_1(x) + u_2(x)) dx = 0.$$

□

We now show that if u_1^0 and u_2^0 are positive and bounded by 1 then u_1 and u_2 stay positive and bounded by 1 on $[0, T]$.

Proposition 4. *Let $(u_1^0, u_2^0) \in L^\infty(\Omega) \times L^\infty(\tilde{\Omega})$ and let T small enough so that a weak solution given by (10) to problem (1) exists. If (u_1^0, u_2^0) are such that*

$$0 \leq u_1^0 \leq 1, \quad 0 \leq u_2^0 \leq 1,$$

then for almost any $t \in [0, T]$

$$0 \leq u_1(t, x) \leq 1, \quad 0 \leq u_2(t, x) \leq 1.$$

In addition

$$0 \leq v(t, x) \leq \frac{1}{\eta} (\gamma_1 + \gamma_2), \quad \text{for } x \in \Omega.$$

Therefore the weak solution (10) exists for almost any $t \in (0, +\infty)$.

Proof. First observe that if u_1 is positive then since u_2^0 is positive the function u_2 is positive almost everywhere. Actually multiplying (1b) by $u_2^- = \max(0, -u_2)$ and integrating by parts implies

$$\frac{1}{2} \partial_t \|u_2^-(t, \cdot)\|_{L^2(\tilde{\Omega})}^2 = -d_2 \|\nabla u_2^-\|_{L^2(\tilde{\Omega})}^2 - \lambda \int_{\tilde{\Omega}} u_1 u_2^- + \lambda u_1 (u_2^-)^2 \leq \lambda M \| (u_2^-)^2 \|_{L^2(\tilde{\Omega})},$$

hence u_2^- equal zero by Gronwall's lemma. Similarly, if u_1 is positive, then since u_2 is therefore also positive we infer that v is positive by multiplying (1c) by v^- and integrating by parts.

Prove now that $u_1^- = \max(0, -u_1)$ vanishes too. Multiply (1a) by u_1^- and integrate by parts to obtain for almost any $t \in [0, T]$:

$$\begin{aligned} \frac{1}{2} \partial_t \|u_1^-(t, \cdot)\|_{L^2(\Omega)}^2 &\leq -d_1 \|\nabla u_1^-(t, \cdot)\|_{L^2(\Omega)}^2 + \lambda(1 + M) \|u_1^-(t, \cdot)\|_{L^2(\tilde{\Omega})}^2 \\ &\quad + \chi^0 \left| \int_{\Omega} u_1^- \frac{v}{1 + |v|} (1 - u_1^-) \nabla v \nabla u_1^- dx \right|. \end{aligned}$$

Moreover applying estimate (9) to v implies

$$\begin{aligned} \left| \int_{\Omega} u_1^- (1 - (u_1 + u_2)) \nabla v \nabla u_1^- dx \right| &\leq C_{\Omega} t^{1/4} \|\gamma_1 u_1(t, \cdot) + \gamma_2 \mathbf{1}_{\tilde{\Omega}} u_2(t, \cdot)\|_{L^\infty(\Omega)} \\ &\quad \times \int_{\Omega} u_1^-(t, x) |1 - u_1^-(t, x)| \nabla u_1^-(t, x) dx \\ &\leq C_{\Omega} T^{1/4} M (\gamma_1 + \gamma_2) (1 + 2M) \int_{\Omega} |u_1^-(t, x)| \nabla u_1^-(t, x) dx \\ &\leq \tilde{C} T^{1/4} \left(\frac{1}{4\alpha} \|\nabla u_1^-\|_{L^2(\Omega)}^2 + \alpha \|u_1^-\|_{L^2(\Omega)}^2 \right) \end{aligned}$$

by Cauchy-Schwarz estimates and the well-known Peetre's inequality with $\alpha > 0$ large enough. Thus since $|s|/(1+|s|) \leq 1$ for any $s \in \mathbb{R}$ we infer

$$\partial_t \|u_1^-(t, \cdot)\|_{L^2(\Omega)}^2 \leq \alpha \tilde{C} T^{1/4} \|u_1^-(t, \cdot)\|_{L^2(\Omega)}^2.$$

Gronwall's lemma implies therefore that

$$\|u_1^-(t, \cdot)\|_{L^2(\Omega)}^2 = 0,$$

since $u_1^-(0, \cdot)$ equals zero.

Prove now that $u_2 \leq 1$. Let $U_2 = u_2 - 1$:

$$\partial_t U_2 = \Delta U_2 - \lambda u_1 U_2,$$

hence multiplying by $U_2^+ = \max(0, U_2)$ the above equation and since $U_2^+(0, \cdot) = 0$ we infer that U_2 vanishes everywhere thanks to Gronwall's lemma, and therefore $u_2 \leq 1$.

Similarly let

$$U_1 = u_1 - 1.$$

Then U_1 satisfies

$$\partial_t U_1 = d_1 \Delta U_1 - \lambda \mathbb{1}_{\tilde{\Omega}}(1 - u_2)(U_1 + 1) + \chi^0 \nabla \cdot \left((U_1 + 1) \frac{v}{1 + |v|} U_1 \nabla v \right), \quad \text{in } \Omega, \quad (12)$$

Once again multiply (12) by $U_1^+ = \max(U_1, 0)$ and integrate by parts to obtain

$$\begin{aligned} \frac{1}{2} \partial_t \left(\|U_1^+\|_{L^2(\Omega)}^2 \right) &= -d_1 \|\nabla U_1^+\|_{L^2(\Omega)}^2 - \lambda \int_{\tilde{\Omega}} (1 - u_2) U_1^+ (U_1^+ + 1) dx \\ &\quad - \chi^0 \int_{\Omega} (U_1^+ + 1) \frac{v}{1 + |v|} U_1^+ \nabla v \cdot \nabla U_1^+ dx. \end{aligned}$$

Since $1 - u_2$ is positive and using Cauchy-Schwarz estimate and Peetre inequality for α large enough (as used above to prove that $u_1 \geq 0$) implies that

$$\partial_t \left(\|U_1^+\|_{L^2(\Omega)}^2 \right) \leq \alpha C \|U_1^+\|_{L^2(\Omega)}^2.$$

Therefore Gronwall lemma implies that U_1^+ vanishes almost everywhere in $(0, T) \times \Omega$ hence $u_1 \leq 1$.

To obtain the positivity of v , first multiply (1c) by v^- and integrate by part to infer, since u_1 and u_2 are positive that:

$$\partial_t \|v^-\|_{L^2(\Omega)}^2 \leq 0.$$

Then the function $V = v - \eta^{-1}(\gamma_1 + \gamma_2)$ satisfies

$$\partial_t V = \Delta V - \eta V + \gamma_1(u_1 - 1) + \gamma_2(u_2 - 1).$$

Since $\gamma_1(u_1 - 1) + \gamma_2(u_2 - 1) \leq 0$, we infer that V^+ identically vanishes after multiplication and integration by parts, hence

$$0 \leq v \leq \eta^{-1}(\gamma_1 + \gamma_2).$$

From the implicit representation integral of u_1 and u_2 we deduce easily that if T_M is the maximal time of existence, then there exists a sequence $(t_n)_{n \in \mathbb{N}}$ tending to T_M , with $t_n < T_M$ such that

$$\lim_{n \rightarrow +\infty} \|u_1(t_n, \cdot)\|_{L^\infty} = +\infty,$$

hence u_1 and u_2 exists for almost any $t \in (0, +\infty)$ by contraposition. \square

Theorem 2.1 is an easy consequence of the above results.

The following result is a straightforward consequence of proposition 4. It ensures that the mass of the cells tends to concentrate on the micropatterns.

Corollary 2. *Let $(u_1^0, u_2^0) \in L^\infty(\Omega) \times L^\infty(\tilde{\Omega})$ such that*

$$0 \leq u_1^0 \leq 1, \quad 0 \leq u_2^0 \leq 1,$$

and let (u_1, u_2) the weak solution to problem (1). Then

$$\begin{aligned} 0 &\leq \int_{\Omega} u_1(t, x) dx \leq \int_{\Omega} u_1(0, x) dx, \\ \int_{\tilde{\Omega}} u_2(0, x) dx &\leq \int_{\tilde{\Omega}} u_2(t, x) dx \leq |\tilde{\Omega}|. \end{aligned}$$

4 Numerical results

We provide now numerical scheme that are used to compute problem (1), and then we show simulation that corroborate the experimental results.

4.1 Approximation of the problem

We consider a cartesian mesh (composed by quadrilaterals). We discretize the model using finite volume method [9] and we use an implicit Crank-Nicolson scheme for the time discretization. We solve the model using a decoupled approach [15]. In particular, the first equation is split into advection and diffusion parts. Let us recall the expression of this equation :

$$\partial_t u_1 = d_1 \Delta u_1 - \lambda \mathbb{1}_{\tilde{\Omega}} u_1 (1 - u_2) - \nabla \cdot (\chi(u_1, v) u_1 \nabla v) \text{ in } \Omega. \quad (13)$$

To simplify the notations we define A and B as:

$$A(u_1, u_2) = d_1 \Delta u_1 - \lambda \mathbb{1}_{\tilde{\Omega}} u_1 (1 - u_2), \quad \text{and} \quad B(u_1, v) = \nabla \cdot (\chi(u_1, v) u_1 \nabla v).$$

Let us denote the time step by Δt , set $t^n = n\Delta t$ and let (u_1^n, u_2^n, v^n) be the solution at the time t^n . At each time step we first solve the diffusive part :

$$\frac{\tilde{u}_1^{n+1} - u_1^n}{\Delta t} = \frac{1}{2} (A(\tilde{u}_1^{n+1}, u_2^{n+1}) + A(u_1^n, u_2^n)).$$

For all the diffusive terms, the spatial discretization is handled by a centered finite volume scheme, all the species being computed at the centre of each element of the mesh. We then solve the advection part :

$$\frac{u_1^{n+1} - \tilde{u}_1^{n+1}}{\Delta t} = \frac{1}{2} (B(u_1^{n+1}, v^{n+1}) + B(\tilde{u}_1^{n+1}, v^n)).$$

The high order WENO 5 (Weighted Essentially Non-Oscillatory) finite difference scheme introduced in [24] and improved in [19] has been used to approach the convective term. These solvers are implemented in the academic library eLYSe¹.

For the numerical computations, we consider a bounded domain $\Omega = [0, L] \times [0, L]$, with $L > 0$. Initially endothelial cells are randomly distributed on the computational domain.

In the following the initial conditions writes as follows

$$u_1^0 = \mathbb{1}_{\Omega \setminus \tilde{\Omega}} u^0, \quad u_2^0 = \mathbb{1}_{\tilde{\Omega}} u^0, \quad (14)$$

where u^0 is a function of $x \in \Omega$. Hence at the initial time the support of u_1 and u_2 are disjoint.

¹<http://www.math.u-bordeaux1.fr/~saut/>

4.2 Mathematical behavior of the model

In this paragraph we present numerical results illustrating the good mathematical behavior of our model. We want to check the properties of the model, when the maximal density on the adhesive area is reached. We consider a domain $\Omega = [0, 1] \times [0, 1]$ and meshes composed by 100×100 quadrilaterals. The domain is composed by a unique adhesive area (cf Fig. 2).

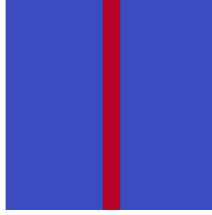


Figure 2: Geometry of the micropattern.

At the initial time the cells are uniformly distributed meaning u^0 of (14) is constant. We consider two different values of u^0 :

$$u^0 = \begin{cases} 0.08, \\ 0.25. \end{cases}$$

We plot the results along the axis $\{y = 0.5\}$ in order to have a profile of the distribution of u_1 and u_2 in the domain. The densities u_1 along the axis at different time steps are given by Fig. 3 and the densities u_2 at the same time steps are represented in Fig. 4.

When considering $u^0 = 0.08$, the maximal density on the adhesive area is never reached. We observe that u_1 is decreasing, while u_2 is increasing with respect to the time. In the second case, $u^0 = 0.25$, the maximal density for u_2 is reached for $t = 0.3$. As expected the migration stops and no more movement are observed. These simulations show that a minimum amount of endothelial cells is needed at initial time in order to reach an optimal concentration on the strips at the end of the experiment. If this initial concentration is too small the final density of endothelial cells is suboptimal.

4.3 Behavior on realistic benchmarks

We now provide simulations in realistic configurations. Therefore throughout this subsection the function u^0 of (14) is a random spatial distribution between 0 and 1 using a normal distribution.

4.3.1 Behavior on thin strips

We first consider a micropattern composed by six thin adhesive areas (in red on Fig.5(b)).

The simulation Fig. 6, represents the total density of endothelial cells ($u = u_1 + u_2$) at times 0.3 (in Fig 6(a)) and 1.0 (in Fig 6(b)) obtained for the following set of parameters: $d_1 = d_2 = \chi^0 = \gamma_2 = 1, \gamma_1 = 0.5, \lambda = 100$.

The figure Fig. 7 shows the behavior of v for the same set of parameters.

We obtain a good agreement with the expected evolution. Indeed, the density of the cells on the adhesive areas increases in time, whereas outside it becomes very small. Cells are stucked

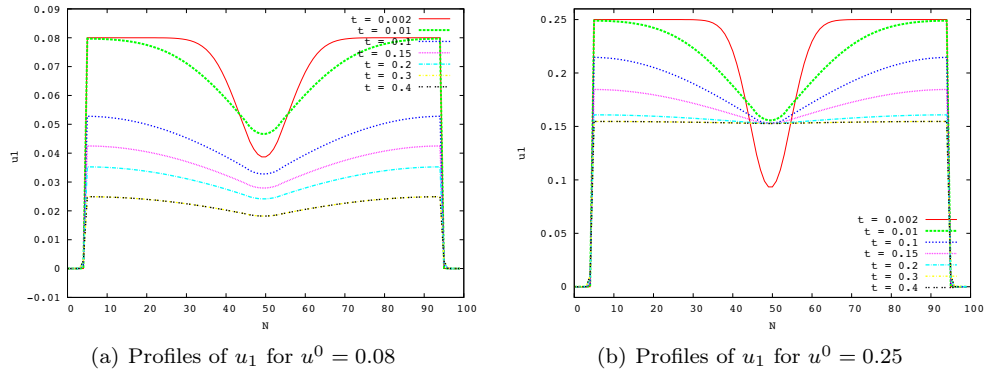


Figure 3: Profiles of $u_1(t, x, y = 0.5)$ at different time steps for two different initial conditions.

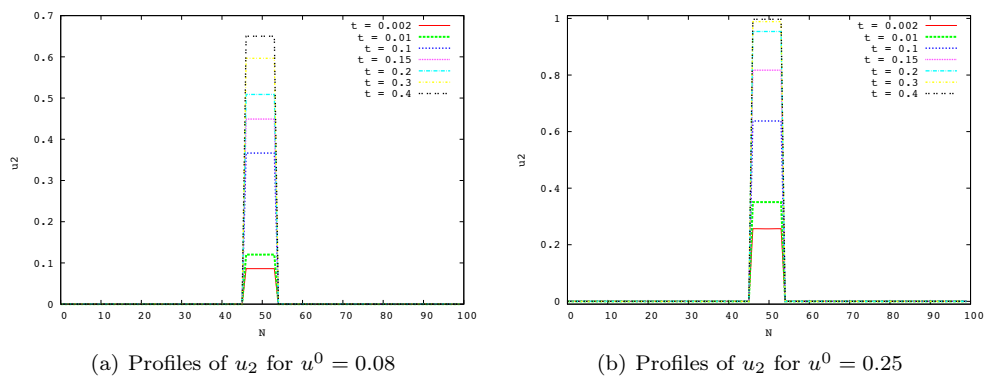


Figure 4: Behavior of $u_2(t, x, y = 0.5)$ at different time steps.

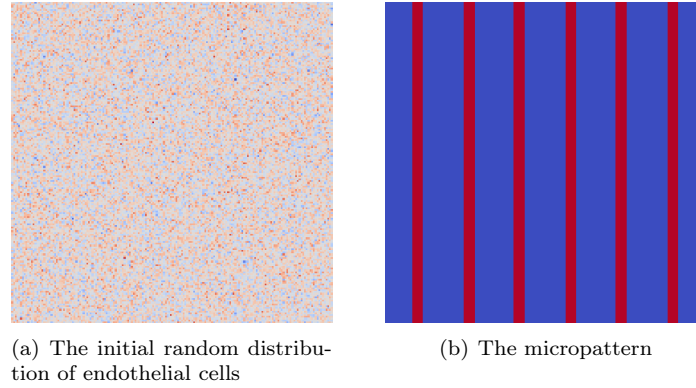


Figure 5: Initial setup: endothelial cells (left) and adhesion substrat (right).

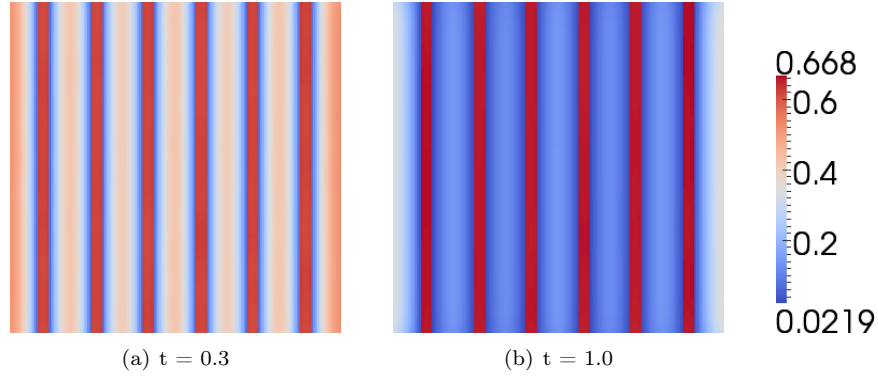


Figure 6: The density of endothelial cells u at two different time steps for $d_1 = d_2 = \chi^0 = \gamma_2 = 1, \gamma_1 = 0.5, \lambda = 100$.

on the strips and stop moving once they are over them. As a consequence the density of the attractant on the strips also increases.

4.3.2 Behavior on large strips

We now consider a domain composed by two large strips. The geometry is presented in Fig.8(b)

In Fig. 9, we present the total density of endothelial cells ($u = u_1 + u_2$) at times 0.3 (in Fig. 9(a)) and 1.0 (in Fig. 9(b)) obtained for the choice of parameters : $d_1 = d_2 = \chi^0 = \gamma_2 = 1, \gamma_1 = 0.5, \lambda = 100$.

In Fig. 10, we present the behavior of v for the same choice of parameters at time $t = 0.3$ and $t = 0.6$.

As previously we observe a behavior in good agreement with the experiments. When considering two large adhesive areas the velocity of the migration is smaller than for a large number of thin strips. Indeed at the time step $t = 1.0$ we observe that with thin strips the migration seems

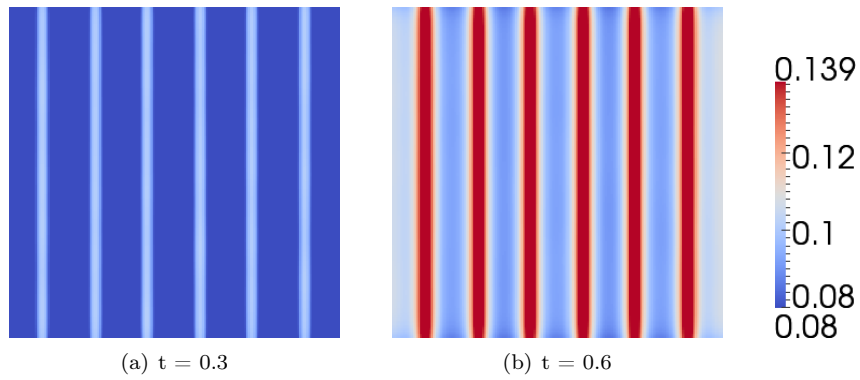


Figure 7: The density v at two different time steps for $d_1 = d_2 = \chi^0 = \gamma_2 = 1, \gamma_1 = 0.5, \lambda = 100$.

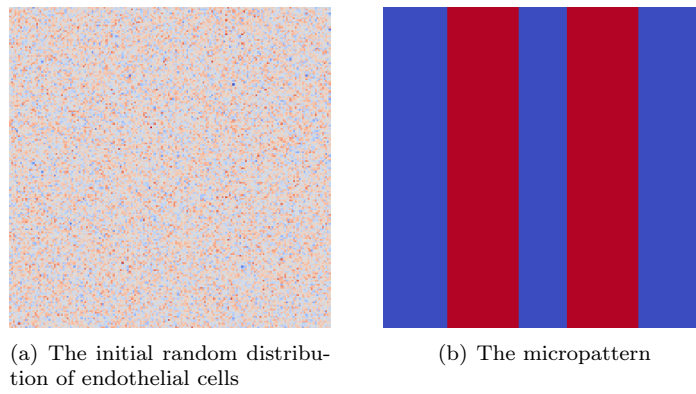


Figure 8: Initial setup: endothelial cells (left) and patterns (right).

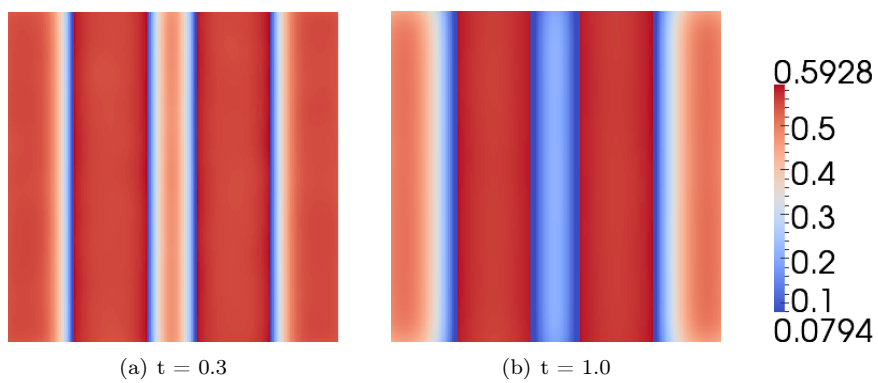


Figure 9: The density of endothelial cells u at two different time steps for $d_1 = d_2 = \chi^0 = \gamma_2 = 1, \gamma_1 = 0.5, \lambda = 100$

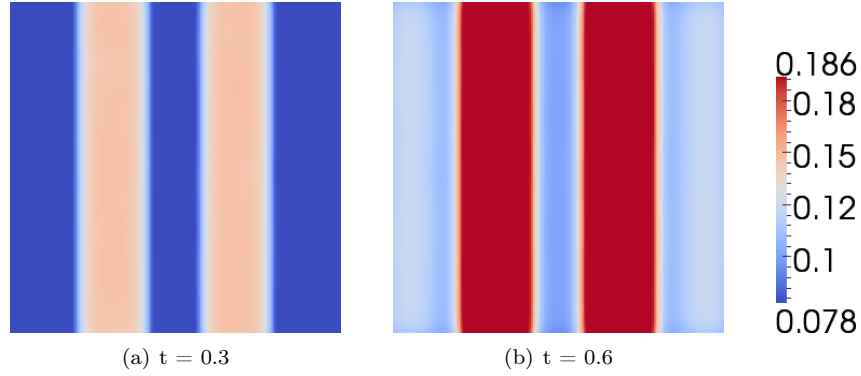


Figure 10: The density v at two different time steps for $d_1 = d_2 = \chi^0 = \gamma_2 = 1, \gamma_1 = 0.5, \lambda = 100$

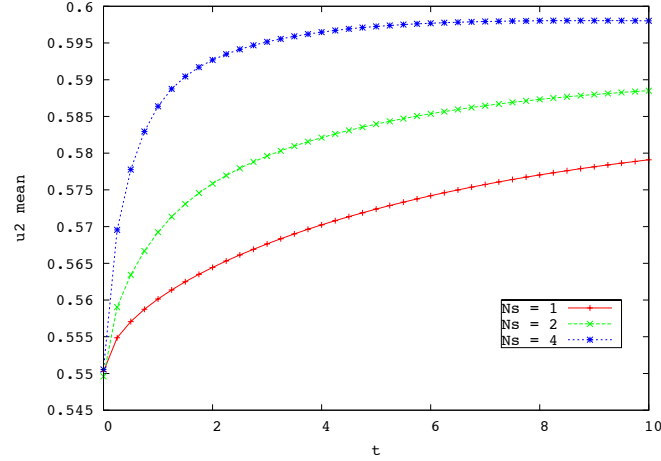


Figure 11: The average of the density u_2 in term of time for different number of strips

to be more advanced than in the case with large strips. This could be explained by the fact this last case some cells are far away from a strip and their migration toward the strips take more time.

4.3.3 Influence of the number of strips on the migration

We want to study the influence of the geometry on the migration. We set the surface of the adhesive domain, and let the number of strips, N_s , vary. The average of u_2 in term of the time for $N_s = 1, 2$, and 4 is presented in Fig. 11 .

We observe that when considering four strips the migration is quicker. Moreover the mean density reached is higher, which corroborates the experiments.

5 Conclusion

In this paper a macroscopic model for endothelial cells migration is presented. Its major biological assumption is that cells are not actively attracted by the adhesion patterns but just adhere on it and try to gather.

Mathematically, mass conservation and global existence is shown. Numerically, the model behaves in good agreement with the biological knowledge. Despite the lack of active attraction by the adhesion patterns, the non-washed out endothelial cells end up on the patterns. We have observed two facts that have been reported by the experiments:

- 1) For a given surface of active principle the process of cell migration is more efficient with a large number of thin strips than with a small number of large strips.
- 2) There exists a minimum value of the initial density of endothelial cells to impose in order to have an optimal cell migration towards the active principle.

We therefore believe that this model is a first step towards better understanding of cell migration on micropatterns, the long-term goal being optimal designing of patterns in order to build biological tissues.

References

- [1] A. Anderson and M. Chaplain. Continuous and discrete mathematical models of tumor-induced angiogenesis. *Bulletin of Mathematical Biology*, 60(5) : 857–899, 1998.
- [2] K. Anselme, P. Davidson, A.M. Popa, M. Giazzon, M. Liley, L. Ploux, The interaction of cells and bacteria with surfaces structured at the nanometre scale, *Acta Biomaterialia*, 6: 3824–3846, 2010
- [3] P. Biler and T. Nadzieja. Existence and nonexistence of solutions for a model of gravitational interaction of particles. I. *Colloq. Math.* 66 : 319–334, 1993.
- [4] A. Blanchet, J. Dolbeault and B. Perthame. Two dimensional Keller–Segel model : optimal critical mass and qualitative properties of the solution. *Electron. J. Differential Equations*, 44 : 1–33, 2006.
- [5] P. Carmeliet and M. Tessier–Lavigne, Common mechanisms of nerve and blood vessel wiring. *Nature*, 436 : 193–200, 2005
- [6] C.S Chen, M. Mrksich, S. Huang, G.M. Whitesides and D.E. Ingber, Geometric control of cell life and death. *Science* 276(5317):1425–1428, 1997.
- [7] L.E. Dike, C.S. Chen, M. Mrksich, J. Tien, G.M. Whitesides, D.E. Ingber, Geometric control of switching between growth, apoptosis, and differentiation during angiogenesis using micropatterned substrates. *In Vitro Cell. Dev. Biol.*, 35 : 441–448, 1999.
- [8] J. Dolbeault and B. Perthame. Optimal critical mass in the two dimensional Keller–Segel model in \mathbb{R}^2 . *C. R. Math. Acad. Sci. Paris*, 339(9) : 611–616, 2004.
- [9] R. Eymard, T. Gallouet, R. Herbin, *Finite Volume Methods*, Handbook of Numerical Analysis, P.G Ciarlet, J.L Lions eds, 2007.
- [10] A. Folch, M. Toner, Microengineering of cellular interactions. *Annu. Rev. Biomed. Eng.*, 2:227–256, 2000.

- [11] J. Folkman and C. Haudenschild . Angiogenesis *in vitro*. Nature, 288 : 551–6, 1980.
- [12] H. Gajewski and K. Zacharias, Global behavior of a reaction-diffusion system modelling chemotaxis. Math. Nachr., 195(1) : 77–114, 1998.
- [13] T. Hillen and K.J. Painter, A user’s guide to PDE models for chemotaxis. J. Math. Biol, 58(1–2) : 183–217, 2008.
- [14] D. Horstmann, The nonsymmetric case of the Keller-Segel model in chemotaxis: some recent results. Nonlinear differ. equ. appl. 8(4) : 399–423, 2001.
- [15] W. Hundsdorfer and J.G. Verwer, *Numerical solution of time-dependent advection-diffusion-reaction equations*. Springer Series in Comput. Math. 33, Springer, 2003.
- [16] Y. Ito, Surface micropatterning to regulate cell functions. Biomaterials, 20:(23/24) 2333–2342, 1999
- [17] R.K. Jain, Molecular regulation of vessel maturation. Nat Med, 9:685–93, 2003.
- [18] R.K. Jain, P. Au, J. Tam, D.G. Duda, D. Fukumura, Engineering vascularized tissue. Nat Biotechnol, 23 : 821–3, 2005
- [19] G.S. Jiang and C.W Shu, Efficient implementation of weighted ENO schemes, J. of Computational Physics, 126 : 202–228, 1996.
- [20] M. Kamei, W.B. Saunders, K.J. Bayless, L. Dye, G.E. Davis and B.M. Weinstein, Endothelial tubes assemble from intracellular vacuoles *in vivo*, Nature 442 : 453–456, 2006.
- [21] E.F. Keller, L.A. Segel, Traveling band of chemotactic bacteria: a theoretical analysis, Journal of Theo. Biol., 30(2) : 235–248, 1971.
- [22] Y. Lei, M. Rémy, O. Zouani, C. Chollet; L. Ramy, C. Chanseau, and M.C. Durrieu, Micropatterning of polyethylene terephthalate with RGD peptides for induction of endothelial cell alignment and morphogenesis, Biomaterials, submitted.
- [23] Y. Lei, O. Zouani, M. Remy, C. Ayela, M.C. Durrieu, Mimicking angiogenesis by SVVYGLR peptide micropatterning, Biomaterials, submitted 2012
- [24] X.D. Liu, S. Osher, and T. Chan. Weighted essentially non-oscillatory schemes. Journal of Computational Physics, 115(1):200–212, 1994.
- [25] B. Lubarsky and M.A. Krasnow. Tube morphogenesis: making and shaping biological tubes. Cell 112 : 19–28, 2003.
- [26] R.M. Nerem Tissue engineering: the hope, the hype, and the future. Tissue Eng 12 : 1143–50, 2006.
- [27] D.V. Nicolau, T. Taguchi, H. Taniguchi, H. Tanigawa and S. Yoshikawa, Patterning neuronal and glia cells on light-assisted functionalized photoresists. Biosens. Bioelectron, 14(3): 317–325, 1999.
- [28] Z.K. Otrock, R.A. Mahfouz, J.A. Makarem and A.I. Shamseddine. Understanding the biology of angiogenesis: review of the most important molecular mechanisms. Blood Cells Mol Dis, 39 : 212–20, 2007.

-
- [29] E.M Ouhabaz. Analysis of heat equations on domains. London Math. Soc. Monographs Series, Princeton University Press. 31, 2005.
 - [30] C.S. Patlak, Random walk with persistence and external bias, Bull. Math. Biophys., 15 : 311–338, 1953.
 - [31] E.A. Phelps and A.J.Garcia, Engineering more than a cell: vascularization strategies in tissue engineering. Curr Opin Biotechnol, 21 : 704–709, 2010.
 - [32] M.I. Santos and R.L. Reis. Vascularization in bone tissue engineering: physiology, current strategies, major hurdles and future challenges. Macromol Biosci, 10 : 12–27, 2010.
 - [33] T. Senba and T. Suzuki, Chemotactic collapse in a parabolic-elliptic system of mathematical biology. Adv. Differential Equations 6 : 21–50, 2001.
 - [34] Y. Y. Li and M. S. Vogelius, Gradient Estimates for Solutions to Divergence Form Elliptic Equations with Discontinuous Coefficients. Arch. Rational Mech. Anal., 153:91–151, 2000.
 - [35] F.Y Wang and L.Yan, Gradient Estimate on Convex Domains and Application. To appear in AMS. Proc., 2012. (available on arxiv: <http://arxiv.org/abs/1009.1965v2>)



**RESEARCH CENTRE
BORDEAUX – SUD-OUEST**

351, Cours de la Libération
Bâtiment A 29
33405 Talence Cedex

Publisher
Inria
Domaine de Voluceau - Rocquencourt
BP 105 - 78153 Le Chesnay Cedex
inria.fr

ISSN 0249-6399